Conclusions

The 218-nm-enhanced C=O6 stretching band of dGMP provides clear evidence for intramolecular H bonding to the O6 atom from metal-bound H_2O for N7-bound Ni^{2+} and *cis*-$(NH_3)_2Pt^{2+}$. When a second G is bound to the Pt, this interaction is abolished, and the C=O6 stretch increases in frequency due to polarization; a larger increase is seen when N7 is protonated. Polarization effects are also seen in frequency and/or intensity changes for several of the guanine ring modes. The sugar-conformation-sensitive guanine modes at 682/666 and 855/864 cm^{-1} indicate an equilibrium mixture of C2′-endo and C3′-endo conformations in the metal complexes, reflecting partial association of the 5′-monophosphate group with Ni^{2+}-bound H_2O molecules but a ring-polarization effect of bound *cis*-$(NH_3)_2Pt^{2+}$. These inferences about the details of the metal–dGMP structures in dilute aqueous solution illustrate the power of the UVRR technique in monitoring the chemical environment of nucleic acid bases.

Acknowledgment. We thank Professors Jan Reedijk and Luigi Marzilli for helpful discussions. This work was supported by NIH Grant GM 25158.

Contribution from the Department of Chemistry,
The University of Houston—University Park, Houston, Texas 77004

Electrochemistry of Iron Porphyrins under a CO Atmosphere. Interactions between CO and Pyridine

C. Swistak and K. M. Kadish*

Received August 19, 1986

The electrochemistry of (TPP)FeCl and (TPP)$FeClO_4$ were investigated in pyridine and in CH_2Cl_2 under a CO atmosphere. Five types of Fe(II) complexes and two types of Fe(I) complexes were spectrally and electrochemically identified. The Fe(II) complexes were (TPP)Fe, $[(TPP)FeCl]^-$, $[(TPP)Fe(CO)Cl]^-$, $(TPP)Fe(py)_2$, and (TPP)Fe(py)(CO) while the Fe(I) complexes were $[(TPP)Fe]^-$ and $[(TPP)Fe(CO)(py)]^-$. An overall oxidation/reduction scheme was formulated for the electrode reactions in pyridine and CH_2Cl_2 under a CO atmosphere. In addition, the kinetics for several ligand displacement reactions were investigated for complexes of Fe(III), Fe(II), and Fe(I) and formation constants for the addition of one or two CO molecules to $[(TPP)FeX]^-$ or (TPP)Fe in CH_2Cl_2 were calculated.

Introduction

The electrochemistry of synthetic iron porphyrins in pyridine and in pyridine/dichloromethane mixtures has been reported by a number of laboratories.[1,2] In the presence of pyridine, the Fe(III)/Fe(II) potentials of (P)FeX (where P is the porphyrin macrocycle and X is an anion other than ClO_4^-) are shifted positively from values obtained in noncomplexing media. At the same time potentials for the Fe(II)/Fe(I) reaction of (P)Fe are shifted negatively from those for reduction of the same complex in a nonbonding solvent. For example, values of $E_{1/2}$ for the first reduction of (TPP)FeX in CH_2Cl_2 (where TPP is the dianion of tetraphenylporphyrin) range between −0.19 V ($X = Br^-$) and 0.47 V vs. SCE ($X = F^-$). Under the same solution conditions, $E_{1/2}$ for the second reduction ranges between −1.06 and −1.07 V vs. SCE for (TPP)FeX complexes where $X = ClO_4^-$, Br^-, Cl^-, or N_3^-. The second reduction of (TPP)FeF is more difficult and occurs at −1.50 V vs. SCE in CH_2Cl_2, 0.1 M (TBA)ClO_4.[3] In contrast, the same porphyrins in pyridine containing 0.1 M (TBA)ClO_4 have $E_{1/2}$ values that range between 0.15 and 0.17 V (first reduction) and between −1.48 and 1.51 V (second reduction).[3] The invariant $E_{1/2}$ values are indicative of the fact that pyridine has replaced the counterion on Fe(III) so that the same six-coordinate $[(TPP)Fe(py)_2]^+$ species exists in solution.[1-3] Also, the increase in stabilization of iron(II) in pyridine (with respect to oxidation or reduction in CH_2Cl_2) is consistent with the fact that large binding constants are found for pyridine addition to (TPP)Fe(II) while much smaller interactions of pyridine occur with (TPP)FeX and no interaction occurs with $[(TPP)Fe^I]^-$.

Bis(pyridine) adducts are invariably formed with iron(II) porphyrins and values of $\beta_2 > 10^8$ have been calculated for (TPP)Fe in CH_2Cl_2 or benzene.[4,5]

$$(TPP)Fe + 2py \rightleftarrows (TPP)Fe(py)_2 \qquad (1)$$

Large binding constants may also be observed for complexation of pyridine by (P)FeX, but this will depend upon the nature of the anionic counterion, X^-, which will compete for the Fe(III) binding site. For example, values of $\beta_2 \approx 10^{7.5}$ are obtained for formation of $[(TPP)Fe(py)_2]^+X^-$ (reaction 2) when the metalloporphyrin is (TPP)$FeClO_4$.[5] On the other hand, much smaller binding constants are obtained when the porphyrin is (TPP)FeCl[6] or (TPP)FeF.[3]

$$(TPP)FeX + 2py \rightleftarrows [(TPP)Fe(py)_2]^+X^- \qquad (2)$$

Very little interaction occurs between the Fe(I) center of $[(TPP)Fe]^-$ and pyridine. It was long thought that nitrogenous bases and specificially pyridine could not bind to the iron(I) state of metalloporphyrins[1,2] but recent low-temperature ESR studies show this not to be the case.[7]

The above example of how pyridine binding affects iron porphyrin redox potentials is not limited to cases where the complexed ligand is a nitrogenous base. Similar examples of potential shifts upon ligand binding have been provided for iron(III) and iron(II) porphyrins containing bound sulfur donor ligands[8,9] as well as for complexation of the iron porphyrins with diatomic molecules such as NO, CS, CSe, O_2, or CO.[1,2] Substantial positive shifts of Fe(II) oxidation potentials also occur after complexation of a given synthetic iron(II) porphyrin with diatomic molecules such as NO, CS, and CSe, and for these later complexes the air-stable state of the porphyrin contains Fe(II).[10,11] This is in contrast to other

(1) See: Kadish, K. M. In *Iron Porphyrins, Part 2*; Lever, A. B. P., Gray, H. B., Eds.; Addison-Wesley: Reading, MA, 1983; pp 161–249.
(2) See: Kadish, K. M. *Prog. Inorg. Chem.* **1986**, *34*, 435–605.
(3) Bottomley, L. A.; Kadish, K. M. *Inorg. Chem.* **1981**, *20*, 1348.
(4) Brault, D.; Rougee, M. *Biochemistry* **1974**, *13*, 4591.
(5) Kadish, K. M.; Bottomley, L. A. *Inorg. Chem.* **1980**, *19*, 832.
(6) (a) Kadish, K. M.; Bottomley, L. A. *J. Am. Chem. Soc.* **1977**, *99*, 2380. (b) Satterlee, J. D.; La Mar, G. N.; Frye, J. S. *J. Am. Chem. Soc.* **1976**, *98*, 7275. (c) Walker, F. A.; Lo, M. W.; Ree, M. T. *J. Am. Chem. Soc.* **1976**, *98*, 5552.
(7) Srivatsa, G. S.; Sawyer, D. T.; Boldt, N. J.; Bocian, D. F. *Inorg. Chem.* **1985**, *24*, 2123.
(8) Wilson, G. S. *Bioelectrochem. Bioenerg.* **1974**, *1*, 172.
(9) Mashiko, T.; Marchon, J. C.; Musser, D. T.; Reed, C.; Kastner, M. E.; Scheidt, W. R. *J. Am. Chem. Soc.* **1979**, *101*, 365.

0020-1669/87/1326-0405$01.50/0

synthetic iron porphyrins where Fe(III) is most often the air-stable oxidation state in the complex.[1,2]

Detailed electrochemistry has been reported for (TPP)Fe and (OEP)Fe (OEP = the dianion of octaethylporphyrin) bound with NO,[12] CS,[10,13] or CSe,[14] but far less information is available on O_2[15] and CO[16-18] adducts of Fe(II). It is known, however, that $(P)Fe^{II}$ will form both mono and bis adducts of CO in nonbonding media[19-21] (reactions 3 and 4) and that no interaction occurs

$$(P)Fe + CO \rightleftarrows (P)Fe(CO) \quad (3)$$

$$(P)Fe(CO) + CO \rightleftarrows (P)Fe(CO)_2 \quad (4)$$

between CO and $[PFe^{III}]^+$ or $(P)Fe^{III}X$. The binding of CO by Fe(I) has been debated for some years,[22,23] but recent evidence shows that CO binding by Fe(I) can occur for certain porphyrins with amide groups in the protective chain.[18]

Our laboratory has also investigated the interaction of CO with iron(I) porphyrins and we have observed that CO binding can occur for nonsterically hindered complexes such as $[(TPP)Fe]^-$. This reaction does not occur in CH_2Cl_2, but room-temperature binding of CO is observed in solutions of pyridine. These reactions are reported in the present paper. In addition, we report the first electrochemistry of six-coordinate iron(II) porphyrins where one of the axial ligands is CO and the other is either pyridine or Cl^-. The former complex was observed in neat pyridine while the latter complex was obtained in CH_2Cl_2 containing 0.1 M (TBA)Cl. Both solutions were under a CO atmosphere. Similar electroreduction mechanisms were observed for $(TPP)FeClO_4$ and (TPP)FeCl in pyridine under CO, and the electronic absorption spectra of the resulting Fe(II) and Fe(I) products are reported.

Experimental Section

Chemicals. (TPP)FeCl and $(TPP)FeClO_4$ were synthesized by literature methods[24,25] while (TPP)FeBr, $(TPP)FeN_3$, and (TPP)FeF were synthesized by acid hydrolysis of the μ-oxo dimer. High-purity-grade carbon monoxide gas was purchased from Linde. Pyridine (py) was refluxed over CaH_2 and distilled prior to use under an argon atmosphere. Unless mentioned otherwise, the solvent contained 0.1 M tetra-*n*-butylammonium perchlorate ($(TBA)ClO_4$) as supporting electrolyte. This salt was purchased from Eastman Chemical Co., recrystallized from ethyl alcohol, dried under high vacuum, and stored at 40 °C under vacuum. All potentials were measured vs. a saturated calomel electrode (SCE) as well as against the ferrocene/ferrocenium (Fc/Fc^+) couple. Ferrocene was purchased from Aldrich Chemical Co.

Instrumentation. Cyclic voltammetric measurements were made on a Bioanalytical System BAS-100 electrochemistry system, and current–voltage curves were recorded on a HIPLOT DMP-40 plotter. A three-electrode geometry was utilized. This consisted of either a platinum button or a mercury–gold amalgam working electrode, a platinum-button counter electrode and a commercial saturated calomel electrode (SCE) as the reference electrode. This latter electrode was separated from the bulk of the solution by a bridge filled with solvent and supporting electrolyte. Total volume utilized was 5–10 mL, and the porphyrin concentrations were maintained between 7×10^{-4} and 10^{-3} M.

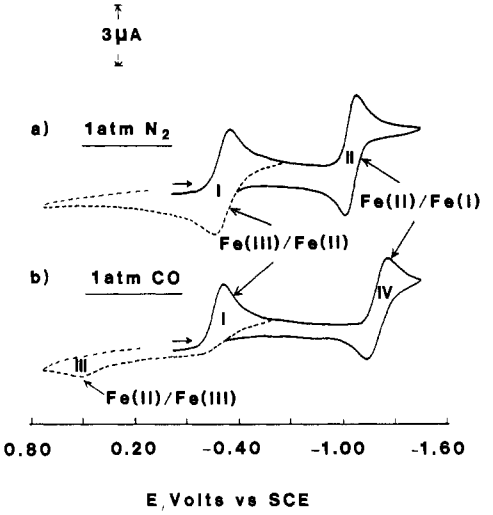

Figure 1. Cyclic voltammograms of (TPP)FeCl in CH_2Cl_2, 0.1 M $(TBA)ClO_4$: (a) under N_2; (b) under CO. Scan rate = 0.20 V/s.

Thin-layer spectroelectrochemical measurements were performed with a PAR Model 173 voltammetric analyzer coupled with a Tracor Northern 1710 holographic optical spectrometer/multichannel analyzer to obtain time-resolved spectral data. Spectra resulted from signal averaging a minimum of 100 sequential spectral aquisitions. Each acquisition represented a single spectrum from 290 to 920 nm simultaneously recorded by a silicon diode array detector with a resolution of 1.2 nm/channel. The utilized vacuum-tight thin-layer cell design has been described in the literature.[26] Sweep rates for thin-layer spectroelectrochemistry were 5 mV/s or below, and a commercial saturated calomel electrode was used as the reference electrode.

A Matheson Model 8250 modular dyna-blender and flow meter were used to deliver a nitrogen/carbon monoxide mixture of known concentration. Partial pressures between 0.01 and 1 atm were possible with this apparatus. As the vapor pressure of pyridine is low, the percentage of CO was considered to be identical with the partial pressure in CO. However, for measurements in dichloromethane the vapor pressure of the solvent (381.6 mmHg at 23 °C) was subtracted from the total pressure in calculating the partial pressure of CO.

Results and Discussion

Reduction of (TPP)FeCl in CH_2Cl_2 under a CO Atmosphere. Figure 1 illustrates cyclic voltammograms for the reduction of (TPP)FeCl under N_2 and under CO. Under both conditions there are two reductions, which correspond to an Fe(III)/Fe(II) and an Fe(II)/Fe(I) transition, respectively. The reductions of (TPP)FeCl in CH_2Cl_2 under N_2 are chemically and electrochemically reversible and have been well described in the literature.[1-3]

The Fe(III)/Fe(II) reduction under N_2 (process I, Figure 1a) occurs at $E_{1/2} = -0.31$ V vs. SCE while that of Fe(II)/Fe(I) (process II, Figure 1a) is located at $E_{1/2} = -1.05$ V vs. SCE. Both processes are electrochemically reversible to quasi-reversible under an N_2 atmosphere. However, under a CO atmosphere the reduction of (TPP)FeCl is chemically irreversible in that the reoxidation of Fe(II) is not directly coupled to the reduction. An irreversible reduction peak is still observed at $E_p = -0.32$ V, but this peak is coupled to an irreversible oxidation (process III) at $E_p = 0.53$ V. At the same time, the second reduction of (TPP)FeCl has shifted from $E_{1/2} = -1.05$ V under 1 atm of N_2 to $E_{1/2} = -1.21$ V under 1 atm of CO. The reduction is labeled as process IV in Figure 1b.

Virtually no change occurs in the shape or potential of current–voltage curves for the reduction of (TPP)FeCl as a function of CO pressure. In contrast, half-wave potentials for the reduction

(10) Buchler, J. W.; Kokisch, W.; Smith, P. D. *Struct. Bonding (Berlin)* **1978**, *34*, 79.
(11) Bottomley, L. A.; Olson, L.; Kadish, K. M. *Adv. Chem. Ser.* **1982**, *No. 201*, 279.
(12) Lançon, D.; Kadish, K. M. *J. Am. Chem. Soc.* **1983**, *105*, 5610.
(13) Bottomley, L. A.; Deakin, M. R.; Gorce, J.-N. *Inorg. Chem.* **1984**, *23*, 3563.
(14) Gorce, J.-N.; Bottomley, L. A. *Inorg. Chem.* **1985**, *24*, 1431.
(15) (a) Dolphin, D.; James, B. R.; Welborn, H. C. *Adv. Chem. Ser.* **1983**, *No. 201*, 563. (b) Welborn, C. H.; Dolphin, D.; James, B. R. *J. Am. Chem. Soc.* **1981**, *103*, 2869.
(16) Gurira, R.; Jordan, J. *Anal. Chem.* **1981**, *53*, 864.
(17) Brown, G. M.; Hopf, F. R.; Meyer, T. J.; Whitten, D. G. *J. Am. Chem. Soc.* **1975**, *97*, 5385.
(18) Croisy, A.; Lexa, D.; Momenteau, M.; Savéant, J. M. *Organometallics* **1985**, *4*, 1574.
(19) Wayland, B. B.; Mehne, L. F.; Swartz, J. *J. Am. Chem. Soc.* **1978**, *100*, 2379.
(20) Strauss, H.; Holm, R. H. *Inorg. Chem.* **1982**, *21*, 863.
(21) (a) Rougee, M.; Brault, D. *Biochem. Biophys. Res. Commun.* **1973**, 1364. (b) Rougee, M.; Brault, D. *Biochemistry* **1975**, *14*, 4100.
(22) Collman, J. P.; Sorrell, T. N.; Dawson, J. H.; Trudel, J. R.; Bunnenberg, E.; Djerassi, C. *Proc. Nat. Acad. Sci. U.S.A.* **1976**, *73*, 6.
(23) Mashiko, T.; Reed, C. A.; Haller, K. J.; Scheidt, W. R. *Inorg. Chem.* **1984**, *23*, 3192.
(24) Adler, A. D.; Longo, F. R.; Kampas, F.; Kim, J. *J. Inorg. Nucl. Chem.* **1970**, *32*, 2443.
(25) Reed, C. A.; Mashiko, T.; Bentley, S. P.; Kastner, M. E.; Scheidt, W. R.; Spartalier, K.; Lang, G. *J. Am. Chem. Soc.* **1979**, *101*, 2948.
(26) Lin, X. Q.; Kadish, K. M. *Anal. Chem.* **1985**, *57*, 1498.

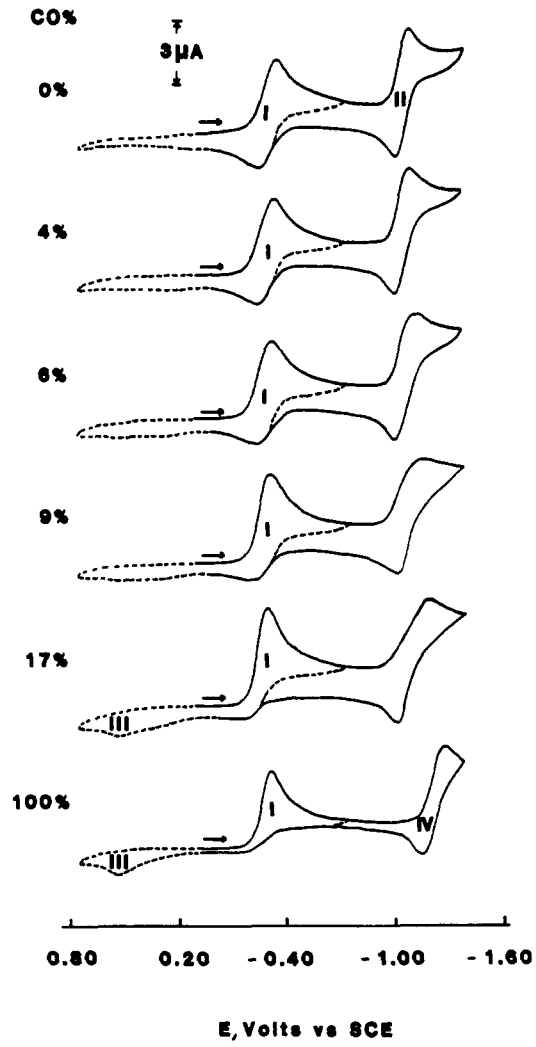

Figure 2. Cyclic voltammograms of (TPP)FeCl in CH_2Cl_2, 0.1 M $(TBA)ClO_4$, recorded at a scan rate of 0.20 V/s in solutions containing various CO/N_2 mixtures.

of Fe(II) (processes II and IV) systematically shift in a negative direction with an increase in the CO partial pressure. This is illustrated by the cyclic voltammograms in Figure 2 as well as by the plot of $E_{1/2}$ for the Fe(II)/Fe(I) process vs. CO pressure shown in Figure 3a.

Figure 2 illustrates cyclic voltammograms of (TPP)FeCl in CH_2Cl_2, 0.1 M $(TBA)ClO_4$ under various N_2/CO gas mixtures. Peak potentials for the first reduction (process I) under CO are shifted to potentials slightly more positive than those under an N_2 atmosphere. At the same time currents for the reoxidation coupled to process I have decreased in magnitude while a new peak (process III) has appeared at more positive potentials. The currents for the reoxidation initially at $E_{1/2} = -0.31$ V continue to decrease with increase of the CO partial pressure, and under a full CO atmosphere there is no reoxidation peak present at these potentials. Under these conditions process III occurs at $E_p = 0.53$ V.

The reduction of (TPP)FeCl under N_2 involves a chemical reaction following electron transfer[3] (an EC mechanism), and there is an equilibrium between (TPP)Fe and $[(TPP)FeCl]^-$ as the final reduction product.[27] The data in Figure 2 indicates that an EC mechanism also occurs under a CO atmosphere. Under these conditions there is no reoxidation peak coupled to the initial reduction process I, and the chemical reaction following reduction of Fe(III) involves the binding of CO by Fe(II).

The number of ligands bound to neutral and reduced (TPP)-FeCl has often been determined from plots of $E_{1/2}$ vs. log [L].[1,2]

(27) Kadish, K. M.; Rhodes, R. K. *Inorg. Chem.* **1983**, *22*, 1090.

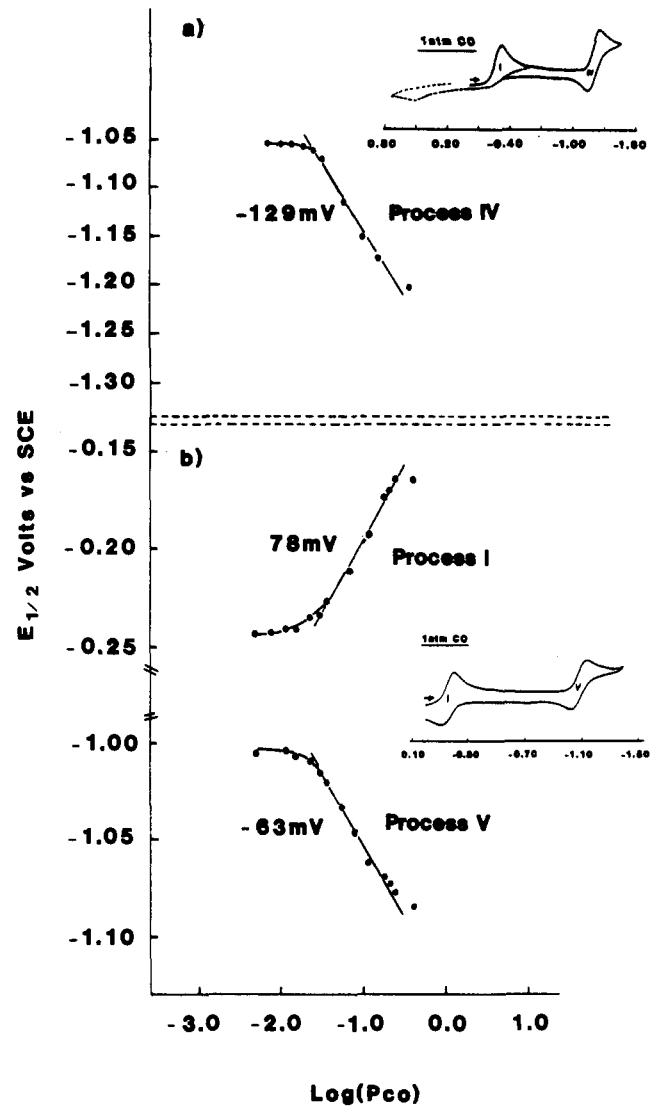

Figure 3. Plot of $E_{1/2}$ vs. log P_{CO} for (a) the second reduction of (TPP)FeCl in 0.1 M $(TBA)ClO_4$ and (b) the first and second reduction of (TPP)FeCl in 0.1 M (TBA)Cl. Insets illustrate the cyclic voltammograms (scan rate = 0.20 V/s) of (TPP)FeCl under 1 atm of CO in each of the two supporting electrolyte solutions.

For the case of CO as an axial ligand the appropriate plot would be $E_{1/2}$ vs. log P_{CO}. Virtually no change occurs in E_{pc} for process I or process III as P_{CO} is increased. This suggests that the binding of CO to Fe(II) and the loss of CO from reoxidized Fe(III) (Process III) do not occur on the time scale of the initial one-electron-reduction/oxidation step. In contrast, significant negative shifts in $E_{1/2}$ occur for the Fe(II)/Fe(I) process as a function of CO partial pressure. This is shown in Figure 3a, which was constructed by using the type of data given in Figure 2.

The Fe(II)/Fe(I) potential is independent of CO pressure up to log P_{CO} values of ~ -2.0, but a Nerstian slope of -129 mV per 10-fold change in P_{CO} is obtained between log $P_{CO} = -2.0$ and -0.2 (see Figure 3a). This slope is consistent with $(TPP)Fe(CO)_2$ as the reactant and $[(TPP)Fe]^-$ as the products of the electrode reaction[1,2] (eq 5).

$$(TPP)Fe(CO)_2 + e^- \rightleftarrows [(TPP)Fe]^- + 2CO \qquad (5)$$

The above data are also consistent with the overall binding of two CO molecules to (TPP)Fe in CH_2Cl_2, 0.1 M $(TBA)ClO_4$, and an overall formation constant of $K_1K_2 = 19.5 \times 10^6$ M^{-1}. This value is given in Table I and compares favorably with the overall binding constant of 9.2×10^6 M^{-1} obtained in toluene.[19] The value of K_1K_2 also compares favorably with formation constants for the addition of two CO molecules to (OEP)Fe in toluene[20] ($K_1K_2 = 7.6 \times 10^6$ M^{-2}) and to (DPDME)Fe in benzene[21] (11.0×10^6 M^{-2}).

Table I. Formation Constants for CO Binding by (TPP)Fe and [(TPP)FeCl]$^-$

reaction	solvent	$10^{-4}K_1$, M^{-1}	$10^{-2}K_2$, M^{-1}	$10^{-6}K_1K_2$, M^{-2}	ref
(TPP)Fe + 2CO ⇄ (TPP)Fe(CO)$_2$	CH_2Cl_2[a]			19.5[c]	*d*
	toluene	6.6	1.40	9.2	19[e]
[(TPP)FeCl]$^-$ + CO ⇄ [(TPP)Fe(CO)Cl]$^-$	CH_2Cl_2[b]	7.0[c]			*d*

[a] In solutions of 0.1 M (TBA)ClO_4. [b] In solutions of 0.1 M (TBA)Cl. [c] Formation constants determined electrochemically and are good to ±25%. [d] This work. Formation constants determined by electrochemical methods. [e] Formation constants determined by spectrophotometric methods.

Table II. Spectral Data for Fe(II) and Fe(I) Complexes in CH_2Cl_2 and Pyridine at Room Temperature

metal oxidn state	absorbing compd	solvent	supporting electrolyte (0.1 M)	atmosphere (1 atm)	λ_{max}, nm ($\epsilon \times 10^{-3}$)				ref
Fe(II)	(TPP)Fe	$EtCl_2$	(TBA)ClO_4	N_2	537 (9)				27
	[(TPP)FeCl]$^-$	$EtCl_2$	(TBA)Cl	N_2	530 sh	570 (12.0)	610 (8.4)		27
	[(TPP)Fe(CO)Cl]$^-$	CH_2Cl_2	(TBA)Cl	CO	536 (13.2)	612 sh			*b*
	(TPP)Fe(CO)$_2$	toluene		CO	~554[a]	~591[a]			19
	(TPP)Fe(CO)	toluene		CO	518[a]				19
	(TPP)Fe(py)$_2$	pyridine	(TBA)ClO_4	N_2	530 (10.6)	562 (2.7)			*b*
	(TPP)Fe(py)(CO)	pyridine	(TBA)ClO_4	CO	530 (10.7)	561 sh	585 sh	617 sh	*b*
Fe(I)	[(TPP)Fe(py)(CO)]$^-$	pyridine	(TBA)ClO_4	CO	530 (6.5)	696 (4)	809 (0.82)		*b*
	[(TPP)Fe]$^-$	pyridine	(TBA)ClO_4	N_2	533 (8.0)	648 sh	713 (3.6)		*b*

[a] Extrapolated from spectra in Figure 4, ref 19. [b] This work.

The binding of CO by Fe(II) results in a positively shifted irreversible Fe(II) ⇄ Fe(III) oxidation (process III) and a negatively shifted reversible Fe(II) ⇄ Fe(I) reduction. The data also indicates that (TPP)Fe(CO)$_2$ is reoxidized to give a transient [(TPP)Fe(CO)$_2$]$^+$ species before generation of [(TPP)Fe]$^+$ or (TPP)FeX as the ultimate oxidation product. Thus, both the reduction of (TPP)FeCl and the oxidation of (TPP)Fe(CO)$_2$ under a CO atmosphere are formulated as electrochemically reversible electron additions or abstractions that are followed by an irreversible chemical reaction (EC type mechanisms). These analyses are consistent with the shape and potential of the reduction/oxidation peaks ($|E_p - E_{p/2}| = 60$ mV and E_p independent of CO partial pressure) as well as data in the literature regarding CO interactions with synthetic Fe(II) and Fe(III) porphyrins.[10,17,19-21,28,29]

Competition between CO and Cl$^-$ for Fe(II) Complexation. The binding of (TPP)Fe^{II} by anions was first illustrated by Kadish and Rhodes[27] using thin-layer spectroelectrochemistry. The initial reduction of (TPP)FeX generates [(TPP)FeX]$^-$, and this anionic Fe(II) species can be stabilized under conditions of high halide ion concentration. For example, in CH_2Cl_2 containing 0.1 M (TBA)ClO_4, the spectrally observed reduction product of (TPP)FeCl is a mixture of [(TPP)FeCl]$^-$ and (TPP)Fe.

In CH_2Cl_2 containing 0.1 M (TBA)Cl only the five-coordinate [(TPP)FeCl]$^-$ complex is observed. Thus, in the presence of excess Cl$^-$ one might envision the formation of [(TPP)Fe(CO)Cl]$^-$ complexes after electroreduction of [(TPP)FeCl]$^-$ under a CO atmosphere. In this case the CO binding reaction would be given by eq 6, where the two electrode reactions of Fe(III) and Fe(II) are represented as processes I and V, respectively.

$$(TPP)FeCl + CO \underset{I}{\overset{e^-}{\rightleftharpoons}} [(TPP)Fe(CO)Cl]^- \underset{V}{\overset{e^-}{\rightleftharpoons}} (TPP)Fe + Cl^- + CO \quad (6)$$

The theoretical shift of potentials as a function of log P_{CO} for the above two reductions are +60 and −60 mV, respectively. As seen in Figure 3b, experimental slopes of +78 (process I) and −63 mV (process V) are obtained. Most importantly, both the Fe(III)/Fe(II) and the Fe(II)/Fe(I) electrode reactions are reversible (see insert of Figure 3b). The shift in $E_{1/2}$ of −63 mV per 10-fold change in CO pressure for process V (Figure 3b) may be compared to the −129-mV shift in the absence of added Cl$^-$ (Figure 3a) and clearly indicates that only a single CO molecule is lost upon the second reduction of (TPP)FeCl in CH_2Cl_2, 0.1 M (TBA)Cl. Carbon monoxide does not bind to [(TPP)Fe^I]$^-$ in CH_2Cl_2, and thus only one CO can be present on the oxidized complex, which is formulated as [(TPP)Fe(CO)Cl]$^-$. This anionic Fe(II) complex can be formed from [(TPP)FeCl]$^-$ under a CO atmosphere, and the data in Figure 3b indicate a CO binding constant of $K_1 = 7.0 \times 10^4$ M^{-1} in CH_2Cl_2, 0.1 M (TBA)Cl. This value is given in Table I and compares with similar binding constants for the addition of one CO molecule to (TPP)Fe in toluene[19] ($K_1 = 6.6 \times 10^4$ M^{-1}), to (OEP)Fe in toluene[20] ($K_1 = 3.3 \pm 0.5 \times 10^4$ M^{-1}), and to (DPDME)Fe in benzene[20] ($K_1 = 5.0 \pm 0.5 \times 10^4$ M^{-1}). However, the negatively charged [(TPP)Fe(CO)Cl]$^-$ is already six coordinate, and a second CO binding reaction does not occur in CH_2Cl_2 solutions containing 0.1 M (TBA)Cl.

Scheme I

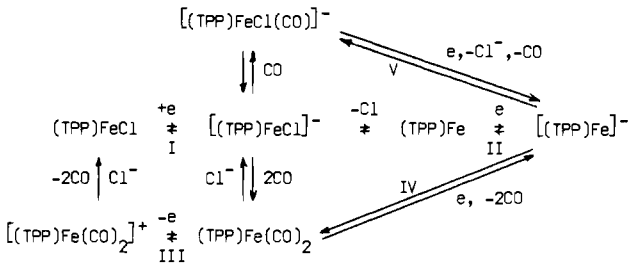

A combination of the data in CH_2Cl_2 containing 0.1 M (TBA)ClO_4 or 0.1 M (TBA)Cl indicates the overall series of electrode reactions shown in Scheme I where the Roman numerals indicate the relevant processes in Figures 1–3.

The initial reduction of (TPP)FeCl in CH_2Cl_2 generates [(TPP)FeCl]$^-$ (process I). This reduction is electrochemically reversible as indicated by the Nerstian-shaped current–voltage curves. However, [(TPP)FeCl]$^-$ is not reoxidized to (TPP)FeCl but rather chemically converts to one of three different Fe(II) products, depending upon the solution conditions.

In the absence of CO and excess chloride ion the ultimate product of (TPP)FeCl reduction is (TPP)Fe. However, in solutions containing 0.1 M (TBA)ClO_4 under a CO atmosphere the ultimate Fe(II) product is (TPP)Fe(CO)$_2$. Finally, in the presence of excess Cl$^-$ and CO the ultimate Fe(II) reduction product is [(TPP)FeCl(CO)]$^-$. This species is fully formed in saturated CO solutions of CH_2Cl_2 containing 0.1 M (TBA)Cl and leads to reversible cyclic voltammograms for both Fe(III)/Fe(II) and Fe(II)/Fe(I).

The only Fe(I) product ever observed in CH_2Cl_2 is [(TPP)Fe]$^-$. This species can be generated by reduction of four different Fe(II) species. In CH_2Cl_2 containing excess Cl$^-$, [(TPP)FeCl]$^-$ will be directly reduced to give [(TPP)Fe]$^-$ (reaction not shown in Scheme I). Alternatively, [(TPP)Fe]$^-$ may be generated from four-coordinate (TPP)Fe (process II), from six-coordinate [(TPP)FeCl(CO)]$^-$ (process V), or from six-coordinate (TPP)Fe(CO)$_2$

(28) Weschler, C. J.; Anderson, D. L.; Basolo, F. *J. Am. Chem. Soc.* **1975**, *97*, 6707.
(29) Stanford, M. A.; Swartz, J. C.; Phillips, T. E.; Hoffman, B. M. *J. Am. Chem. Soc.* **1980**, *102*, 4492.

Table III. Half-Wave and Peak Potentials (V vs. SCE) for the Fe(III)/Fe(II) and Fe(II)/Fe(I) Reactions of (TPP)FeX in CH_2Cl_2 under N_2 and CO

supporting electrolyte	initial compd	Fe(III)/Fe(II) under N_2 $E_{1/2}$ (E_{pc})[a]	Fe(III)/Fe(II) under CO E_{pc}[a]	Fe(III)/Fe(II) under CO E_{pa}[a]	Fe(II)/Fe(I) under N_2 $E_{1/2}$	Fe(II)/Fe(I) under CO $E_{1/2}$
0.1 M TBAP	(TPP)$FeClO_4$	0.22 (0.19)	−0.25	0.54	−1.04	−1.19
	(TPP)FeBr	−0.21[b] (−0.28)	−0.29	0.53	−1.04	−1.21
	(TPP)FeCl	−0.31 (−0.35)	−0.32	0.53	−1.05	−1.21
	(TPP)FeN_3	−0.41 (−0.45)	−0.46	0.26	−1.04	−1.24
	(TPP)FeF	−0.49	−0.48[c]	0.54	−1.50	−1.25[f]
0.1 M (TBA)Br	(TPP)FeBr	−0.24 (−0.29)	−0.27	*d*	−0.99	*e*
0.1 M (TBA)Cl	(TPP)FeCl	−0.24 (−0.27)	−0.16[d]	*d*	−1.01	−1.08

[a] Scan rate = 0.20 V/s. [b] See ref 3 for details on (TPP)FeBr reduction. [c] Reversible $E_{1/2}$ value. [d] Beyond limit of supporting electrolyte oxidation. [e] Wave badly defined. [f] Two other reductions occur at E_{pc} = −1.20 V and $E_{1/2}$ = −1.50 V. The currents for these processes are smaller and the reductions are due to the presence of some (TPP)$Fe(CO)_2$ and $[(TPP)FeF]^-$ in solution.

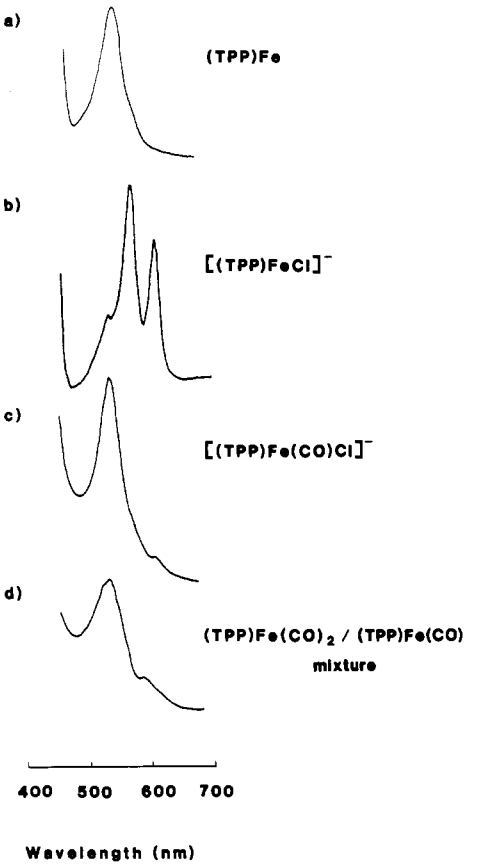

Figure 4. Thin-layer spectra of various Fe(II) species in CH_2Cl_2 after electroreduction of (a) (TPP)$FeClO_4$ in 0.1 M (TBA)ClO_4, (b) (TPP)FeCl in 0.1 M (TBA)Cl, (c) (TPP)FeCl in 0.1 M (TBA)Cl under 1 atm of CO, and (d) (TPP)$FeClO_4$ under 1 atm of CO. The species assigned to each spectrum are given in the figure.

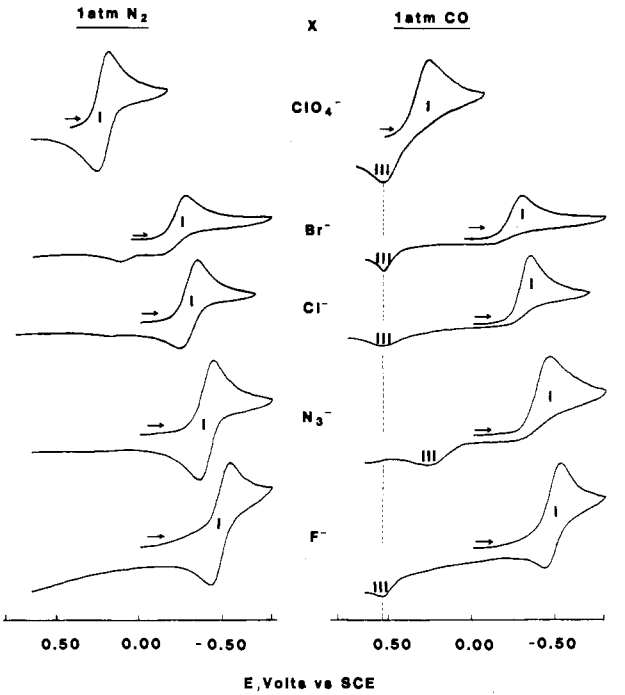

Figure 5. Cyclic voltammograms showing the first reduction of (TPP)FeX (where X = ClO_4^-, Br^-, Cl^-, N_3^-, and F^-) in CH_2Cl_2 under 1 atm of N_2 and under 1 atm of CO.

(process IV). These latter two electrode reactions are shown by the upper and lower pathways in Scheme I.

The binding of both CO and Cl^- to (TPP)Fe^{II} is also indicated by electronic absorption spectra taken in CH_2Cl_2. These data are presented in Figure 4 and Table II, which gives maximum wavelengths and molar absorptivities of each electrogenerated Fe(II) complex. The spectra of (TPP)Fe and $[(TPP)FeCl]^-$ (Figure 4a,b) agree with spectral data in the literature for these two complexes. Four-coordinate (TPP)Fe was generated by controlled-potential reduction of (TPP)$FeClO_4$ in 0.1 M (TBA)ClO_4, while five-coordinate $[(TPP)FeCl]^-$ was generated by reduction of (TPP)FeCl in 0.1 M (TBA)Cl. The former porphyrin complex has a single absorption band at 537 nm while the latter anionic Fe(II) species has two absorption bands at 570 and 610 nm.

The spectrum assigned to $[(TPP)Fe(CO)Cl]^-$ is shown in Figure 4c. This species has a single absorption band in the visible region that is located at 536 nm. The spectrum does not resemble that of $[(TPP)FeCl]^-$ nor is it close to that of (TPP)Fe(CO) or (TPP)$Fe(CO)_2$. The dicarbonyliron(II) spectrum has bands at ~554 and ~591 nm, but this species is not fully formed at room temperature, as indicated by NMR and UV–visible spectra.[19] Thus, although the electrochemistry indicates a complete conversion of (TPP)Fe to (TPP)$Fe(CO)_2$ at the electrode surface, the thin-layer UV–visible spectra indicates a mixture of (TPP)$Fe(CO)_2$ and (TPP)Fe(CO) (which has a band at 518 nm). The room temperature spectrum of this mixture has one broad band between 518 and 560 nm and another smaller band at 589 nm. This spectrum is shown in Figure 4d, and a summary of the spectral details for all of the Fe(II) complexes in CH_2Cl_2 is given in Table II.

Reduction of Other (TPP)FeX Complexes in CH_2Cl_2 under a CO Atmosphere. A similar reduction/oxidation scheme occurs for (TPP)FeX under CO where X = ClO_4^-, Br^-, N_3^-, and F^-. This is illustrated by the data in Figure 5. Figure 5a illustrates the behavior of (TPP)FeX at a Pt electrode under N_2 while Figure 5b shows voltammograms for the same series of compounds under a CO atmosphere. In both cases peak potentials for the first reduction of Fe(III) (labeled process I) shift negatively with increase in strength of the counterion. This is most dramatic for reactions under N_2 and has been described in the literature.[3]

Values of half-wave potentials and peak potentials for (TPP)FeX reduction under N_2 and under a CO atmosphere are listed in Table III. The first reduction peak of (TPP)FeX is not

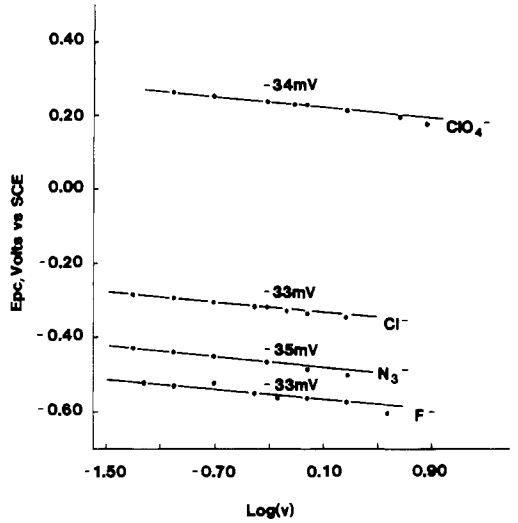

Figure 6. Scan rate dependence on the first reduction peak of (TPP)FeX (where X = ClO_4^-, Cl^-, N_3^-, and F^-) in CH_2Cl_2, 0.1 M (TBA)ClO_4, under 1 atm of CO.

directly coupled to an anodic reoxidation peak under CO for complexes with X = ClO_4^-, Br^-, Cl^-, and N_3^-. However, an oxidation peak at more positive potentials is coupled to the initial reduction process. This peak is labeled as process III and occurs at $E_p = 0.53 \pm 0.01$ V for (TPP)FeX complexes where X = ClO_4^-, Cl^-, Br^-, and F^-. A more negative $E_p = 0.26$ V is found for X = N_3^- (see Table III).

The first reduction of (TPP)FeX is irreversible for all of the complexes except for (TPP)FeF, which appears to be electrochemically reversible under full CO pressure. This is due to the strong competition between F^- and CO for binding to Fe(II) and results in significantly increased concentrations of $[(TPP)FeF]^-$ at the electrode surface. However, there is still an oxidation peak present for $(TPP)Fe(CO)_2$ at $E_p = 0.54$ V.

The counterion bound to Fe(III) initially remains associated after reduction of $(TPP)FeN_3$ and (TPP)FeF in CH_2Cl_2 containing (TBA)ClO_4 but after a short time a mixture of several different Fe(II) products is obtained. The main product of the electrode reaction is $[(TPP)FeX(CO)]^-$ but some $(TPP)Fe(CO)_2$ is also obtained as shown in eq 7, where X = N_3^- and F^-. Evidence for

$$(TPP)FeX + e^- \rightleftarrows [(TPP)FeX]^- \overset{CO}{\rightleftharpoons} [(TPP)Fe(X)(CO)]^- \overset{CO}{\rightleftharpoons} (TPP)Fe(CO)_2 + X \quad (7)$$

the above EC mechanism comes from an evaluation of E_{pc} as a function of scan rate as well as from a spectral monitoring of the reduction products which indicate a mixture of the anionic and neutral six-coordinate Fe(II) species.

The negative shift of E_{pc} as a function of increased scan rate is shown in Figure 6 for the first reduction of (TPP)FeX where X = ClO_4^-, Cl^-, N_3^-, and F^-. The theoretical shift of E_{pc} for an EC mechanism is −30 mV per 10-fold change in log v. The experimental slopes in Figure 6 vary between −33 and −35 mV, confirming the EC mechanism but indicating a small amount of uncompensated IR loss.

Reduction of (TPP)FeCl and (TPP)$FeClO_4$ in Pyridine under a CO Atmosphere. (TPP)FeCl and (TPP)$FeClO_4$ are dissociated in neat pyridine,[5] and the Fe(III) species in solution can be represented as $[(TPP)Fe(py)_2]^+X^-$. Under these conditions the bis(pyridine) complex can be reduced by either two or three electrons, depending upon the type of electrode material. There are two reductions at a Pt electrode, which occur at +0.18 and −1.45 V vs. SCE. A third reduction is not observed on Pt due to the negative cutoff range of the pyridine solvent. In contrast, the first reduction of $[(TPP)Fe(py)_2]^+X^-$ is just at the positive limit of a Hg electrode in pyridine but a second and third reduction of the complex are well-defined on Hg and occur at −1.47 and −1.71 V vs. SCE.

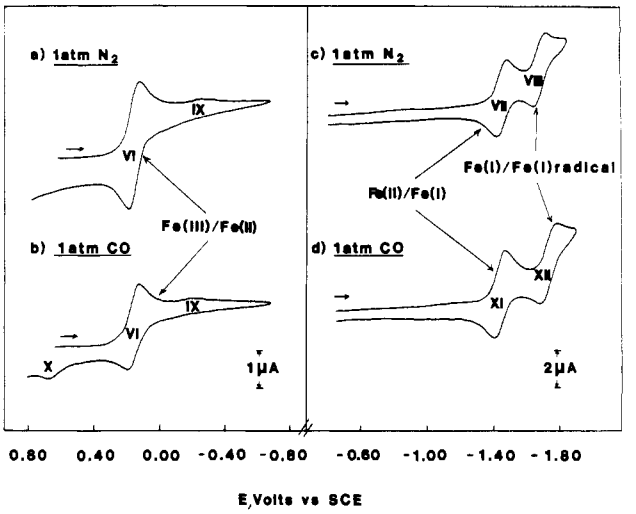

Figure 7. Cyclic voltammograms showing the reduction of (TPP)FeCl in pyridine, 0.1 M (TBA)ClO_4, under the following conditions: (a) under 1 atm of N_2 at a Pt electrode; (b) under 1 atm of CO at a Pt electrode; (c) under 1 atm of N_2 at a Hg electrode; (d) under 1 atm of CO at a Hg electrode.

Voltammograms showing the three electroreductions of $[(TPP)Fe(py)_2]^+Cl^-$ under N_2 are illustrated in Figure 7a,c, and the reactants and products in each of the three electrode reactions are given by eq 8–10. These reactions are assigned as processes VI–VIII in Figure 7.

$$[(TPP)Fe(py)_2]^+ + e^- \rightleftarrows (TPP)Fe(py)_2 \quad (8)$$

$$(TPP)Fe(py)_2 + e^- \rightleftarrows [(TPP)Fe]^- + 2py \quad (9)$$

$$[(TPP)Fe]^- + e^- \rightleftarrows [(TPP)Fe]^{2-} \quad (10)$$

Carbon monoxide will not bind to $[(TPP)Fe(py)_2]^+$ but it will bind to $(TPP)Fe(py)_2$.[29] The kinetics and thermodynamics of CO binding by $(TPP)Fe(L)_2$ have been investigated for Fe(II) complexes containing adducts of Im, 1-MeIm, py, and piperidine. The binding of CO to the bis(nitrogenous base) adduct of Fe(II) is generally described in terms of a preequilibrium involving prior dissociation of one axial ligand followed by a CO addition to the five-coordinate complex.[29] For the case of pyridine as an axial ligand this would correspond to the reaction given by eq 11. The

$$(TPP)Fe(py)_2 \overset{-py}{\rightleftharpoons} (TPP)Fe(py) \overset{CO}{\rightleftharpoons} (TPP)Fe(py)(CO) \quad (11)$$

initial formation of $(TPP)Fe(py)_2$ in pyridine will occur via the electrode reaction given in eq 8, but a reoxidation or a further reduction of the electrogenerated Fe(II) species will involve either $(TPP)Fe(py)_2$, (TPP)Fe(py), or (TPP)Fe(py)(CO) as the reactant. The specific Fe(II) species in solution will depend upon potential scan rate, temperature, and both the kinetics and thermodynamics of each ligand-exchange reaction.

In order to investigate the above competition between CO and py, the reductions of (TPP)FeCl and (TPP)$FeClO_4$ were carried out at various scan rates and temperatures in neat pyridine containing various partial pressures of CO. Examples of two current voltage curves under 1 atm of CO are given by parts b and d of Figure 7. The voltammogram in Figure 7b has a reversible reduction at +0.18 V (peak VI), a small irreversible reduction at −0.26 V (peak IX), and a larger irreversible oxidation at +0.66 V (peak X). The reversible reduction involves the conversion of $[(TPP)Fe(py)_2]^+$ to $(TPP)Fe(py)_2$ (eq 8) while the irreversible reduction process IX is due to reduction of some undissociated six-coordinate (TPP)FeCl(py).

The oxidation process at 0.66 V (peak X) involves an electrochemically reversible oxidation of (TPP)Fe(py)(CO) to give a transient $[(TPP)Fe(CO)(py)]^+$ species at the electrode surface. A similar electrooxidation mechanism has been presented for [EtioI)Fe(CO)(Im) in CH_2Cl_2.[17] The mixed CO/py adduct of

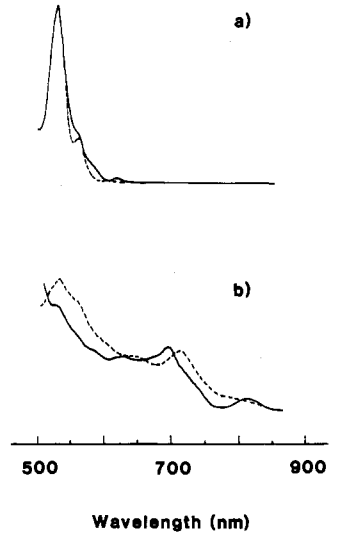

Figure 8. Thin-layer spectra: (a) $(TPP)Fe(py)_2$ (---) and (TPP)Fe(CO)(py) (—); (b) $[(TPP)Fe]^-$ (---) and $[(TPP)Fe(CO)(py)]^-$ (—). The spectra were obtained after the two one-electron controlled-potential reductions of $[(TPP)Fe(py)_2]^+$ in pyridine under N_2 (---) and under CO (—).

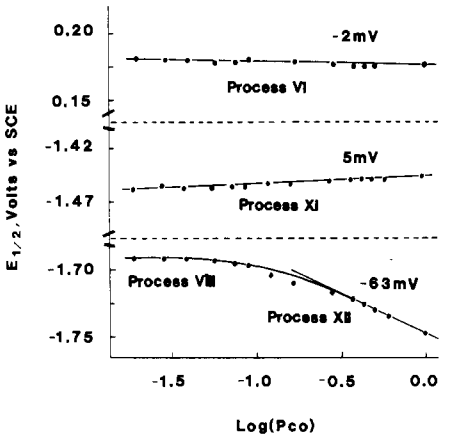

Figure 9. Dependence of $E_{1/2}$ on log P_{CO} for the three reversible electrode reactions of (TPP)FeCl in pyridine, 0.1 M $(TBA)ClO_4$, under a CO atmosphere. Processes VI, VIII, XI, and XII are identified in Figure 7.

Fe(II) is the ultimate product of $[(TPP)Fe(py)_2]^+$ reduction in pyridine, but because $(TPP)Fe(py)_2$ is more easily oxidized ($E_{1/2}$ = 0.18 V) than (TPP)Fe(CO)(py) (E_{pc} = 0.66 V), some reassociation of py will occur prior to electrooxidation (reaction 12).

$$(TPP)Fe(CO)(py) + py \rightleftarrows (TPP)Fe(py)_2 + CO \quad (12)$$

The rate constant for the above reaction is slow ($k < 10^{-6}$ s^{-1} at −79 °C in CH_2Cl_2[28]), but the driving force for this CE type mechanism is the 500-mV difference in oxidation potentials between the two couples.

The second and third reductions of $[(TPP)Fe(py)_2]^+$ under a CO atmosphere occur at −1.45 and −1.76 V (Hg electrode) and can be represented by eq 13 and 14 in solutions of pyridine

$$(TPP)Fe(CO)(py) + e^- \rightleftarrows [(TPP)Fe(CO)(py)]^- \quad (13)$$

$$[(TPP)Fe(CO)(py)]^- + e^- \rightleftarrows [(TPP)Fe]^{2-} + py + CO \quad (14)$$

containing high CO concentrations. Equation 13 is represented by process XI while eq 14 is represented by process XII. The key point in the above equations is that CO binds to the Fe(I) complex. This has been demonstrated for the case of basket-handle porphyrins[18] but has never been observed for the case of simple $[(TPP)Fe]^-$ complexes.

Evidence for CO binding by Fe(II) and Fe(I) comes from the generated thin-layer spectra in pyridine with and without added

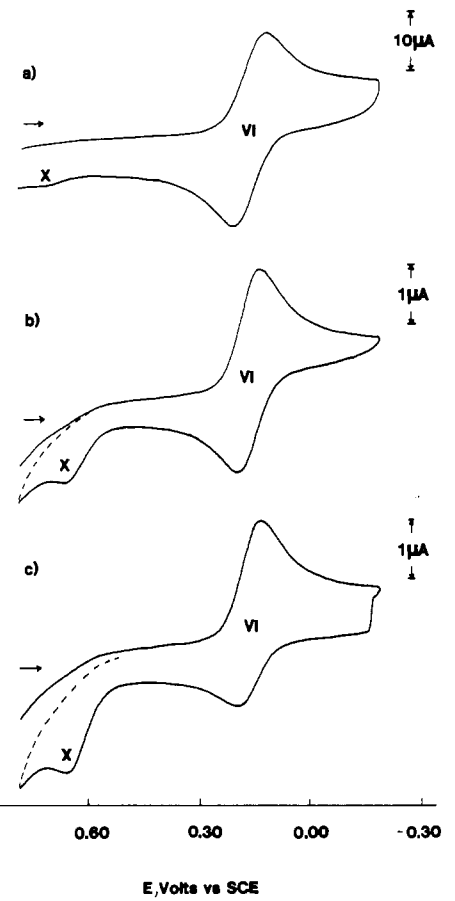

Figure 10. Cyclic voltammograms showing the first reduction of (TPP)$FeClO_4$ in pyridine, 0.1 M $(TBA)ClO_4$: (a) at 10 V/s, (c) at 0.2 V/s, (c) at 0.2 V/s with 40-s hold at −0.16 V/s.

CO (see Figure 8 and Table II for spectral details) as well as from plots of $E_{1/2}$ vs. log P_{CO} in neat pyridine (Figure 9). The first reduction of (TPP)FeCl is reversible in pyridine, and the $E_{1/2}$ for this reduction is independent of CO partial pressure. The Fe(II)/Fe(I) half-wave potentials in pyridine are also independent of CO partial pressure but there is a −63-mV shift in the $E_{1/2}$ vs. log P_{CO} plot for the Fe(I)/Fe(I) anion radical reaction. This later Nerstian slope suggests loss of one carbon monoxide molecule upon formation of the Fe(I) anion radical and strongly implies the formation of $[(TPP)Fe(py)(CO)]^-$.

The formation of $[(TPP)Fe(py)(CO)]^-$ is also implied from thin-layer spectra obtained in the presence and absence of CO. These spectra are shown in Figure 8 and were taken after the two one-electron reductions of $[(TPP)Fe(py)_2]^+$ in pyridine under a CO atmosphere. As seen in this figure (and in Table II, which lists spectral details) there are perceptible spectral differences between the solution under N_2 and that under CO. However, the most clear indication of CO binding to Fe(I) comes from the −63-mV slope in the $E_{1/2}$/log P_{CO} plot of Figure 9. This Nerstian shift can only be accounted for by CO binding to Fe(I). In this regard, it should be noted that CO binding is not totally novel for Fe(I) porphyrins. The binding of carbon monoxide has not been previously observed for $[(TPP)Fe^I]^-$ but other superstructured porphyrins do bind CO, and this reaction is facilitated by a strong donor ligand at the sixth axial position.[18]

Overall Electron-Transfer Mechanism in Pyridine/CO Mixtures. An equilibrium exists between electrogenerated $(TPP)Fe(py)_2$ and (TPP)Fe(py)(CO), and this should be reflected in the relative currents for processes VI and X in Figure 7d. However, both Fe(II) species are electroactive, and for this reason the position of the equilibrium will depend on the applied electrode potential and the potential sweep rate. As a consequence the observed currents for the two oxidation processes will not reflect the actual composition of each species in solution. For example, even though (TPP)Fe(py)(CO) is the final electroreduction product of

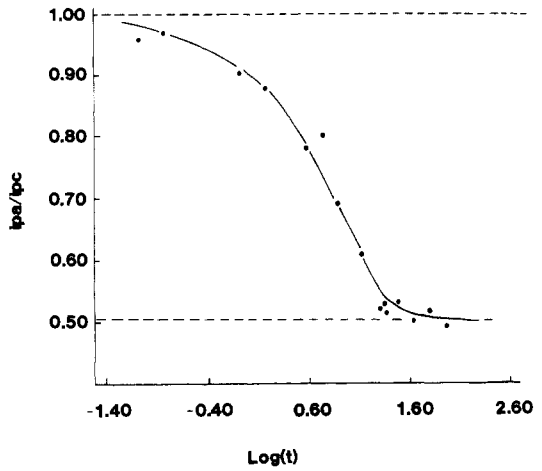

Figure 11. Influence of scan rate and hold time on the reoxidation currents of $[(TPP)Fe(py)_2]ClO_4$ (process VI) in pyridine, 0.1 M $(TBA)ClO_4$, under a CO atmosphere. Data was calculated from voltammograms of the type shown in Figure 10.

$[(TPP)Fe(py)_2]^+$, a single reversible couple can still theoretically be observed at the extremes of very fast or very slow potential scan rates. This is because at fast scan rates there would be no time for CO to replace py on $(TPP)Fe(py)_2$ after its electrochemical generation, and under these conditions only the reaction given by eq 8 will be observed. The same overall reaction should also be observed at extremely slow potential scan rates. This is because $(TPP)Fe(py)_2$ is more easily oxidized than (TPP)Fe(py)(CO), and thus the equilibrium will shift toward $(TPP)Fe(py)_2$ as this more easily oxidized species is consumed at the electrode surface.

The experimental ratio of currents for processes VI and X under different experimental conditions are illustrated by the data in Figures 10 and 11. Figure 10 shows voltammograms obtained under three conditions. At a fast potential scan rate (10 V/s), the ratio of i_{pa}/i_{pc} for process VI is close to 1.0 and there is almost no current associated with process X. However, at 200 mV/s the ratio of i_{pa}/i_{pc} has decreased to 0.81, and higher oxidation currents are observed at $E_p = 0.66$ V. This is shown in Figure 10b. Finally, the value of i_{pa}/i_{pc} decreased to ~0.54 while the currents for Process X increased even further when the potential was scanned through the first reduction at 0.20 V/s but then held at the switching potential for 40 s before the sweep was reversed. This is shown in Figure 10c.

Scheme II

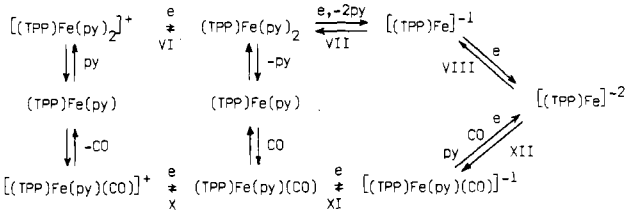

A series of experiments were then carried out in which both the scan rate and the hold time at −0.20 V were varied. Results from these experiments are shown in Figure 11, which plots i_{pa}/i_{pc} vs. log t, where t is measured as the sum of the hold time at −0.20 V plus the time elapsed between $E_{1/2}$ and this switching potential.

As seen in Figure 11, the i_{pa}/i_{pc} ratio varies between 1.0 and 0.50. No current ratios less than 0.50 were obtained, thus indicating that a rapid conversion of (TPP)Fe(CO)(py) to the more easily oxidized $(TPP)Fe(py)_2$ was occurring at the electrode surface.

A combination of these data with those involving reduction of Fe(II) thus leads to the oxidation/reduction mechanism in pyridine/CO mixtures shown in Scheme II. In Scheme II $[(TPP)Fe(py)_2]^+$ is reduced to $(TPP)Fe(py)_2$ (process VI), which then converts to (TPP)Fe(py)(CO) under a CO atmosphere. This latter species can then be reduced to give stable $[(TPP)Fe(py)(CO)]^-$ by process XI or be oxidized to give transient $[(TPP)Fe(py)(CO)]^+$ by process X.

In all cases (TPP)Fe(py)(CO) is the ultimate Fe(II) product in the electroreduction under a CO atmosphere. This is shown by thin-layer spectroscopy (see Table II) and by the fact that there are increased currents for (TPP)Fe(CO)(py) oxidation upon holding the cyclic scan at negative potentials after first electroreducing $[(TPP)Fe(py)_2]^+$ (Figure 10). Finally, in the absence of CO only $[(TPP)Fe]^-$ is electrochemically observed. Furthermore, the product of the third reduction seems to generate $[(TPP)Fe]^{2-}$ under all conditions of pyridine and CO.

Acknowledgment. The support of the National Institutes of Health (Grant GM25172) is gratefully acknowledged.